Astron. Astrophys. 320, 305–318 (1997)

ASTRONOMY AND ASTROPHYSICS

Direct excitation of resonant torsional Alfvén waves by footpoint motions

Michael S. Ruderman[1,2], **David Berghmans**[1,⋆], **Marcel Goossens**[1], **and Stefaan Poedts**[3]

[1] Centre for Plasma Astrophysics, K.U. Leuven, Celestijnenlaan 200 B, B-3001 Heverlee, Belgium
[2] on leave of Institute for Problems in Mechanics, Russian Academy of Sciences, 117526 Moscow, Russia
[3] FOM-Institute for Plasma Physics 'Rijnhuizen', P.O. Box 1207, 3430 BE Nieuwegein, The Netherlands

Received 5 August 1996 / Accepted 1 October 1996

Abstract. The present paper studies the heating of coronal loops by linear resonant Alfvén waves that are excited by the motions of the photospheric footpoints of the magnetic field lines. The analysis is restricted to torsionally polarised footpoint motions in an axially symmetric system so that only torsional Alfvén waves are excited. For this subclass of footpoint motions, the Alfvén and cusp singularities are absent from the analysis which means that resonant coupling between global modes of the loop and localised oscillations is avoided. Instead, the focus is on the resonances due to the finite extent of the loop in the longitudinal direction: at the radii where Alfvén waves travelling back and forth along the length of the loop are in phase with the footpoint motions, the oscillations grow unbounded in ideal MHD. Inclusion of electrical resistivity and viscosity as dissipation mechanisms prevents singular growth and we can look at the steady state in which the energy injected at the photospheric part of the loop is balanced by the energy dissipated at the dissipative layer around the resonance. In this sense, we show that the direct excitation of Alfvén waves by torsionally polarised footpoint motions leads to a very efficient heating mechanism for coronal loops, even without resonant coupling to global modes.

Key words: MHD – Sun: corona; oscillations – waves – methods: analytical

1. Introduction

High resolution observations from space and from the ground give overwhelming evidence that the solar corona is a highly inhomogeneous plasma which is structured by the ubiquitous magnetic field. Since Skylab it is known that the largest contribution to the X-ray emission and to the heating of the solar corona comes from loop like structures in the solar atmosphere. The magnetic loops are viewed as the basic magnetic building blocks of the solar corona. They are curved magnetic flux tubes of increased plasma density which have both ends rooted in the dense photosphere. The high conductivity and the relatively high mass density of the photospheric plasma provide an effective photospheric anchoring of the magnetic field lines. The photospheric footpoints of the magnetic field lines are forced to follow the convective motions of the photospheric plasma. The motions of the footpoints of the magnetic field lines in turn excite MHD waves in the magnetic loops. Arbitrary footpoint motions generate fast and slow magnetosonic waves and Alfvén waves. Due to the steep density gradients at the photospheric edges these MHD waves are reflected back and forth along the length of the loop. The loop then acts as a leaking, resonant cavity for MHD-waves which can be dissipated by various mechanisms and finally heat the loop.

An important property of MHD waves in an inhomogeneous plasma is that individual magnetic surfaces can oscillate with their own Alfvén frequencies. In ideal linear MHD this happens without interaction with neighbouring magnetic surfaces. These local Alfvén oscillations are polarized in the magnetic surfaces and perpendicular to the magnetic field lines. Dissipative effects produce coupling to neighbouring surfaces. For large values of the viscous and magnetic Reynolds numbers as in the solar corona the local Alfvén oscillations are still characterized by steep gradients across the magnetic surfaces.

Excitation of these local Alfvén oscillations provides a means for dissipating wave energy which is far more effecient in a weakly dissipative plasma than classical resisitive or viscous MHD wave damping in uniform plasmas. This can be achieved by means of a global wave that is in resonance with the local Alfvén oscillations of a specific magnetic surface. The resonance condition is that the frequency of the global motion is equal to the local Alfvén frequency of the magnetic surface. The effect is that energy is transferred from the large scale motion to oscillations which are highly localised to the neighbourhood of the Alfvén or cusp singular surface. Due to the small length

Send offprint requests to: M. Goossens
⋆ Research Assistant of the Belgian National Fund for Scientific Research

scales thus generated, dissipation is enhanced by several orders of magnitude over its classical value in a uniform plasma. This ability to absorb a large amount of wave energy even in a weakly dissipative plasma has attracted ample attention. Ionson (1978) proposed resonant absorption of MHD waves as a mechanism for heating magnetic loops in the solar corona. Since this original work, resonant absorption has remained a popular mechanism for explaining the heating of the solar corona (see e.g. Kuperus, Ionson, & Spicer 1981; Ionson 1985; Davila 1987; Hollweg 1990,1991; Goossens 1991; Ofman & Davila 1995).

Most applications of heating by resonant absorption involve lateral driving and an indirect excitation of the localised oscillations. The global waves are supposed to be present either outside the coronal loop and to impinge on the loop or to be present inside the loop. Either way the global wave transfers energy across the magnetic surfaces up to the resonant surface where the frequency of the global wave equals the local Alfvén frequency. In this sense the excitation of the localised oscillations is indirect since we need magnetosonic waves that propagate across the magnetic surfaces to excite them. Numerical simulations have shown that the quasi modes play a fundamental role in this scenario (Poedts, Goossens & Kerner 1989; Steinolfson & Davila 1993; Ofman, Davila & Steinolfson 1995). Tirry & Goossens (1996) identified these quasi modes as eigenmodes of the dissipative MHD equations with the property that their damping rate becomes independent of dissipation in the limit of increasingly small dissipative coefficients. Resonant absorption is most efficient for driving at a frequency that equals the real part of the eigenvalue of a quasi mode. In addition the time evolution of the process is dominated by the quasi mode which manifests itself as the natural oscillation mode of the magnetic loop. For the quasi mode to be present in the analysis the footpoint motions need to have a component normal to the magnetic surfaces (Berghmans, De Bruyne & Goossens 1996). Such footpoint motions excite fast and slow magnetosonic waves and Alfvén waves producing a complicated dynamical system.

A second scenario for the excitation of localised Alfvén oscillations involves driving at the photospheric footpoints of the magnetic field lines. This provides direct excitation of the localised Alfvén oscillations. In an axially symmetric equilibrium an axially symmetric footpoint motion (which bypasses the Alfvén singularity) with a velocity component only in the torsional direction (which avoids the cusp singularity) produces only Alfvén waves which travel back and forth along the loop and are reflected at the photospheric boundaries of the loop by the steep density gradients (Berghmans & De Bruyne 1995). Although classical resonant absorption at the Alfvén or cusp resonance is thus fully excluded from this system, other resonances which are due to the finite geometry of a line-tied loop still play a dominant role. On the radii where the back and forth reflected waves are precisely in phase with the footpoint motion, the waves interfere constructively giving rise to a localised growing oscillation. In this sense, it is possible to drive the localised Alfvén waves directly at the footpoints.

Heating of plasmas by dissipation of localised waves driven by footpoint motions was first studied by Heyvaerts & Priest (1983) in linear MHD in planar geometry. Subsequently it was studied in a numerical investigation by Straus & Lawson (1989). From the numerical work by Straus & Lawson (1989) it transpired that the Alfvén continuum in a line-tied cylindrical plasma differs from that of an untied plasma in the sense that the Alfvén continuum of a line-tied cylinder is independent of the azimuthal component of the equilibrium magnetic field. This result was put on a firm footing by Goedbloed & Halberstadt (1994). These authors then studied the excitation of Alfvén waves (Halberstadt & Goedbloed 1995a,b) driven at the photospheric base of the loop (both sideways and by the footpoints). In a numerical experiment in non-linear resistive MHD, Poedts & Boynton (1996) excited the Alfvén waves directly at the footpoints and found that nonlinear Alfvén waves can dissipate sufficient energy to heat coronal loops without resorting to the resonant coupling to a quasi mode.

The aim of this paper is to gain analytical insight in the direct excitation of resonant Alfvén waves in the context of linear viscous resistive MHD. In addition we obtain a very simple scheme for the accurate computation of resonant Alfvén waves driven by footpoint motions.The ratio of the length to the radius of a coronal loop (the aspect ratio) is large in most cases. This makes it possible to forget about the curvature of the loop and to model the loop in a first approximation as a straight cylinder or a slab of plasma. Our results are for a cylindrical geometry but since the governing equation is formally identical in planar geometry, the results can be easily carried over. We consider an equilibrium state with straight magnetic field lines in the longitudinal z-direction and assume that the equilibrium quantities only depend on the radial coordinate r. We eliminate the Alfvén resonance by an azimuthal symmetric perturbation ($m = 0$) and bypass the cusp resonance by restricting the analysis to footpoint motions polarised in the torsional direction. For the time dependence of the footpoint motion we take a harmonic oscillation with a frequency ω. This enables us to circumvent the time integration of the time dependent equations of linear viscous resistive MHD by considering the steady state of stationary Alfvén waves in which all the perturbed variables oscillate with the frequency ω. If ω lies in the Alfvén continuum, the amplitude of the oscillations at the corresponding resonant magnetic surface is infinite in ideal MHD. Inclusion of dissipation (viscosity and/or finite resistivity) in the analysis removes this singularity. In the solar corona where dissipation is weak, the situation is still reminiscent to the ideal case: the effect of dissipation is negligible everywhere except in a narrow dissipative layer embracing the ideal resonant surface where the amplitudes of oscillations are very large (but finite). Inspired by the SGHR-method of matched asymptotics (Sakurai, Goossens & Hollweg 1991; Goossens, Ruderman & Hollweg 1995; Goossens & Ruderman 1995) we derive an explicit analytical solution for the resonant Alfvén oscillations. Far away from the dissipative layer the driven oscillations are accurately described by the ideal MHD equations which admit an extremely simple analytical solution. The combination of the (dissipative) solution to the dissipative MHD equations in the dissipative layer and the ideal solution provides us with a complete analytical solution for the driven Alfvén oscillations. This

solution gives us physical insight in the problem and provides us with an easy tool for accurate computations of the resonant Alfvén waves. The analytical solutions of the present study are compared with results obtained by numerical integration of the linear dissipative MHD equations in the whole volume of the equilibrium model with a finite element method. The analytic solution is used to obtain expressions for describing the energetics of the system such as the Poynting flux, of which the analytical value is compared with that obtained in the numerical simulation.

The paper is organized as follows. In the next section we describe the equations and the boundary conditions for the driven Alfvén waves, and derive from these a linear equation which governs Alfvén waves. In Sect. 3 we present an asymptotic solution for resonant Alfvén waves which is valid in a weakly dissipative plasma. In Sect. 4 we study the absorption of energy of the footpoint motion due to the damping of resonant Alfvén waves. In Sect. 5 we compare the analytical solutions with the numerical solutions obtained on the basis of the full set of linear resistive MHD equations for a particular case. Sect. 6 gives a short discussion of the theoretical results for the magnetic loops in the solar corona. Finally, in Sect. 7, we summarize the obtained results.

2. Equations and boundary conditions

We use the linearized viscous resistive finite-pressure MHD equations for describing the linear motions superimposed on a static equilibrium:

$$\frac{\partial \rho'}{\partial t} + \nabla \cdot (\rho_0 \mathbf{v}) = 0 \,, \tag{1}$$

$$\rho_0 \frac{\partial \mathbf{v}}{\partial t} = -\nabla p' + \frac{1}{\mu}[(\nabla \times \mathbf{B}_0) \times \mathbf{B}' + (\nabla \times \mathbf{B}') \times \mathbf{B}_0] + \rho_0 \nu \nabla^2 \mathbf{v} \,, \tag{2}$$

$$\frac{\partial \mathbf{B}'}{\partial t} = \nabla \times (\mathbf{v} \times \mathbf{B}_0) + \eta \nabla^2 \mathbf{B}' \,, \tag{3}$$

$$\frac{\partial p'}{\partial t} + \mathbf{v} \cdot \nabla p_0 = \frac{\gamma p_0}{\rho_0} \left(\frac{\partial \rho'}{\partial t} + \mathbf{v} \cdot \nabla \rho_0 \right) . \tag{4}$$

Here ρ_0, p_0, and $\mathbf{B}_0$ denote the equilibrium density, pressure, and magnetic field. We consider a static equilibrium, so that there is no equilibrium velocity. An accent on a quantity denotes the Eulerian perturbation of that quantity. Hence ρ', p', and $\mathbf{B}'$ are the Eulerian perturbations of density, pressure, and magnetic field. $\mathbf{v}$ is the perturbed velocity, μ is the magnetic permeability, ν the kinematic coefficient of viscosity, η the coefficient of magnetic diffusion, and γ the adiabatic index. In spite of the presence of finite resistivity we use an adiabatic Eq. (4) as an approximation for the energy equation. In what follows we only consider Alfvén waves. The equations that describe Alfvén waves are decoupled from the energy equation, so that the exact form of the energy equation is unimportant for the present study.

We consider an equilibrium model with a magnetic field with straight magnetic field lines and let the direction of the z-axis coincide with the direction of the equilibrium magnetic field, so that $\mathbf{B}_0 = B_0 \mathbf{e}_z$, where $\mathbf{e}_z$ is the unit vector of the z axis. We consider a cylindrical geometry (r, φ, z) where all equilibrium quantities depend on r only. The analysis in a Cartesian geometry can be carried out in the same manner and will not be given here. The magnetic field lines are frozen into the dense plasma of the photosphere which in our straightened loop model is situated at $z = 0$ and $z = L$. We assume that the MHD waves are driven by the footpoint motions of the magnetic field lines anchored in the dense photosphere at the position $z = 0$ and assume the dense photosphere at the position $z = L$ immovable. This can be done without any loss of generality because of the principle of superposition for solutions of linear equations.

The objective of the present paper is to study the direct photospheric excitation of linear Alfvén waves that are resonant because of the finite extent of the loop in the longitudinal direction. We want to do this in the simplest possible situation which still contains the basic physics. Hence we aim to avoid complications with coupling of Alfvén waves to global magnetosonic motions which is of obvious interest but would here only obscure the properties of the Alfvén waves. This leads us to restrict the footpoint motions to the azimuthal direction. This class of footpoint motions drives torsional Alfvén waves.

The boundary conditions at $z = 0$ then take the form

$$v_r = 0 \,, \quad v_\varphi = f(t, r) \,, \quad v_z = 0. \tag{5}$$

Here $f(t, r)$ is a prescribed function, and $\mathbf{v} = (v_r, v_\varphi, v_z)$. The assumption that the photosphere is immovable at the position $z = L$ leads to the boundary condition

$$v_r = 0 \,, \quad v_\varphi = 0 \,, \quad v_z = 0. \tag{6}$$

Let us now proceed with the derivation of the equations for v_φ and B'_φ. We start from the azimuthal components of the momentum equation (2) and the induction equation (3). They can be written as

$$\frac{\partial v_\varphi}{\partial t} = -\frac{1}{\rho_0 r} \frac{\partial P'}{\partial \varphi} + \frac{B_0}{\mu \rho_0} \frac{\partial B'_\varphi}{\partial z} + \nu \left[\frac{\partial}{\partial r} \left(\frac{1}{r} \frac{\partial (r v_\varphi)}{\partial r} \right) + \frac{1}{r^2} \frac{\partial^2 v_\varphi}{\partial \varphi^2} + \frac{\partial^2 v_\varphi}{\partial z^2} + \frac{2}{r^2} \frac{\partial v_r}{\partial \varphi} \right] , \tag{7}$$

$$\frac{\partial B'_\varphi}{\partial t} = B_0 \frac{\partial v_\varphi}{\partial z} + \eta \left[\frac{\partial}{\partial r} \left(\frac{1}{r} \frac{\partial (r B'_\varphi)}{\partial r} \right) + \frac{1}{r^2} \frac{\partial^2 B'_\varphi}{\partial \varphi^2} + \frac{\partial^2 B'_\varphi}{\partial z^2} + \frac{2}{r^2} \frac{\partial B'_r}{\partial \varphi} \right] , \tag{8}$$

where $P' = p' + B_0 B'_z / \mu$ is the Eulerian perturbation of the total pressure.

The first and the last terms in the righthand side of Eq. (7) and the last term in the righthand side of Eq. (8) contain a derivative with respect to φ of respectively P', v_r and B'_r. These

terms will couple the Alfvén waves to the slow and fast magnetosonic waves. Since we want to focus our attention exclusively on Alfvén waves we further restrict our analysis to axially symmetric motions where all perturbed quantities are independent of φ. In terms of Fourier decomposition with respect to φ this means that we take the azimuthal wavenumber $m = 0$. This enables us to look for solutions with

$$v_r = 0\,, \quad v_z = 0\,, \quad P' = 0. \tag{9}$$

We assume that viscosity and magnetic diffusion are weak so that they are only important in the narrow dissipative layer embracing an ideal resonant surface. The perturbed quantities undergo fast radial variations close to the ideal resonant point. Hence in the dissipative layer the derivative of the perturbed quantities with respect to r is much larger than that with respect to z. In addition the derivative of a perturbed quantity is also much larger than the perturbed quantity devided by r. This enables us to neglect all terms but the first one in the square brackets in Eqs. (7) and (8), and rewrite these equations for axially symmetric perturbations as

$$\frac{\partial v_\varphi}{\partial t} = \frac{B_0}{\mu\rho_0}\frac{\partial B'_\varphi}{\partial z} + \nu\frac{\partial^2 v_\varphi}{\partial r^2}\,, \tag{10}$$

$$\frac{\partial B'_\varphi}{\partial t} = B_0\frac{\partial v_\varphi}{\partial z} + \eta\frac{\partial^2 B'_\varphi}{\partial r^2}\,. \tag{11}$$

In order to obtain the basic equation for torsional Alfvén waves in terms of v_φ alone we need to eliminate B'_φ from the Eqs. (10) and (11). To that end we first differentiate Eq. (10) with respect to t and use Eq. (11) to get

$$\frac{\partial^2 v_\varphi}{\partial t^2} - v_A^2(r)\frac{\partial^2 v_\varphi}{\partial z^2} = \nu\frac{\partial^3 v_\varphi}{\partial t\partial r^2} + \frac{B_0\eta}{\mu\rho_0}\frac{\partial^3 B'_\varphi}{\partial r^2\partial z}\,. \tag{12}$$

$v_A^2(r) = B_0(r)^2/\mu\rho_0(r)$ is the square of Alfvén velocity. In a non-uniform plasma $v_A(r)$ is a function of position. This will be important for the present discussion of resonant Alfvén waves in line-tied plasmas. We now use Eq. (10) for eliminating B'_φ from Eq. (12). Neglecting the terms that are quadratic in the small quantities ν and η, and also the terms that contain derivatives of equilibrium quantities with respect to r, we finally arrive at the desired equation for torsional Alfvén waves in terms of the azimuthal component of the velocity

$$\frac{\partial^2 v_\varphi}{\partial t^2} - v_A^2(r)\frac{\partial^2 v_\varphi}{\partial z^2} = (\nu+\eta)\frac{\partial^3 v_\varphi}{\partial t\partial r^2}\,. \tag{13}$$

Eq. (13) in combination with the boundary conditions at $z = 0$ and $z = L$ governs the temporal evolution and the spatial variation of linear Alfvén waves in visco-resistive MHD. The righthand term in Eq. (13) is due to dissipation and causes a coupling of different magnetic surfaces. Since dissipation is very weak this coupling will also be weak. In the absence of dissipation the righthand member of Eq. (13) is identically zero and Eq. (13) then describes pure torsional Alfvén waves that live in splendid isolation on a specific magnetic surface without any coupling to the neighbouring magnetic surfaces.

The boundary conditions (5) and (6) now reduce to

$$v_\varphi(r, z = 0, t) = f(r, t) \quad \text{and} \quad v_\varphi(r, z = L, t) = 0\,. \tag{14}$$

The derivation of the equation corresponding to Eq. (13) in planar geometry parallels that of Eq. (13), so that we do not give any details. In a Cartesian coordinate system where the direction of the $x-$axis is the direction of the inhomogeneity of the equilibrium state and the direction of the $z-$axis is the direction of the equilibrium magnetic field lines it suffices to substitute v_y for v_φ and x for r in Eq. (13) and in boundary condition (14).

In the following section we obtain solutions to Eq. (13) and the boundary condition (14), that describe steady oscillations in a magnetic cylinder.

3. Asymptotic solution for stationary standing Alfvén waves

3.1. Fourier decomposition

Instead of solving the full time dependent Eq. (13) for v_φ we look for stationary solutions describing standing Alfvén waves and assume that all perturbed quantities and in particular v_φ are proportional to $\exp(-i\omega t)$ with real ω. This means that we assume that the footpoint motions have driven the loop for a sufficiently long time so that the resonance layer has been build up and a steady state is attained in which the energy injected by the footpoint motions is balanced by the energy dissipated at the resonance layer. In Sect. 3.4 we show that the time necessary to reach the stationary phase of the resonance layer is much shorter than the life time of the loop so that a steady state approach is possible.

Eq. (13) and the boundary conditions (14) can then be rewritten as

$$\omega^2 v_\varphi + v_A^2\frac{\partial^2 v_\varphi}{\partial z^2} = i\omega(\nu+\eta)\frac{\partial^2 v_\varphi}{\partial r^2}\,, \tag{15}$$

and

$$v_\varphi(r, z = 0) = f(r) \quad \wedge \quad v_\varphi(r, z = L) = 0\,, \tag{16}$$

where now v_φ is a function of the two spatial coordinates r and z, but independent of t.

In order to obtain a differential equation with homogeneous boundary conditions it is convenient to introduce the new dependent variable

$$V(r, z) = v_\varphi(r, z) - \left(1 - \frac{z}{L}\right) f(r)\,. \tag{17}$$

In terms of this new unknown variable V equation (15) and boundary conditions (16) take the form

$$\omega^2 V(r, z) + v_A^2(r)\frac{\partial^2 V}{\partial z^2} - i\omega(\nu+\eta)\frac{\partial^2 V}{\partial r^2} = \left(1 - \frac{z}{L}\right) g(r)\,, \tag{18}$$

and

$$V(r, z) = 0 \quad \text{at} \quad z = 0 \quad \wedge \quad \text{at} \quad z = L\,. \tag{19}$$

The effect of the footpoint motions is contained in the function $g(r)$ which appears in the righthand member of equation (18):

$$g(r) = i\omega(\nu+\eta)\frac{d^2 f(r)}{dr^2} - \omega^2 f(r)\,. \tag{20}$$

The homogenous boundary conditions (19) enable us to expand $V(r,z)$ in a Fourier series of the form

$$V(r,z) = \sum_{n=1}^{\infty} V_n(r)\sin\frac{\pi n z}{L}\,. \tag{21}$$

Solving the partial differential Eq. (18) for $V(r,z)$ now requires solving an infinite set of ordinary differential equations with respect to r for the unknown coefficient functions $V_n(r)$. We obtain this infinite set of ordinary differential equations for the unknown coefficient functions $V_n(r)$ by substituting expansion (21) into Eq. (18) and using the expansion

$$1 - \frac{z}{L} = \frac{2}{\pi}\sum_{n=1}^{\infty}\frac{1}{n}\sin\frac{\pi n z}{L} \tag{22}$$

The infinite set of ordinary differential equations for the unknown coefficient functions $V_n(r)$ is given by

$$\left(\omega^2 - \frac{\pi^2 n^2 v_A^2}{L^2}\right)V_n(r) - i\omega(\nu+\eta)\frac{d^2 V_n(r)}{dr^2} = \frac{2g(r)}{\pi n} \tag{23}$$

where $n \in N_0$.

The expansion (22) is valid for all z but $z = 0$. This means that we shall obtain a weak solution to Eq. (18) which has a discontinuous second order derivative with respect to z at $z = 0$. Since from a physical point of view a weak solution is as good as a classic solution (i.e. with a continuous second derivative), there is no need to worry about the validity of expansion (22) at $z = 0$.

3.2. Solution in an ideal plasma

For what follows it is instructive to note that in the set of Eq. (23) dissipation is contained in the righthand side and in the last term of the lefthand side. In the absence of dissipation the last term in the lefthand vanishes and the righthand side reduces to $-\omega^2 f(r)$. In this ideal approximation the set of differential equations for the coefficient functions reduces to a set of algebraic equations

$$\left(\omega^2 - \frac{\pi^2 n^2 v_A^2}{L^2}\right)V_n(r) = \frac{-2\omega^2 f(r)}{\pi n} \tag{24}$$

where $n \in N_0$, which has the solution

$$V_n(r) = \frac{-2\omega^2 L^2 f(r)}{\pi n[\omega^2 L^2 - \pi^2 n^2 v_A^2(r)]}\,. \tag{25}$$

In the absence of dissipation ($\nu = \eta = 0$) there is even no need to use a Fourier series expansion with respect to z. Eq. (15) is an ordinary differential equation with respect to z and contains r only as a parameter. The solution to this equation that satisfies the boundary conditions (16) is

$$v_\varphi = f(r)\frac{\sin[\omega(L-z)/v_A(r)]}{\sin[\omega L/v_A(r)]}\,. \tag{26}$$

A straightforward Fourier transformation of solution (26) shows that the two solutions, namely that given by Eqs. (17), (21), and (25), and that given by Eq. (26), are equal.

Solutions (25) and (26) are physically acceptable if

$$\forall n \in N_0 \quad \wedge \quad \forall r \in [0 \;\; R] : \omega^2 \neq \frac{\pi^2 n^2 v_A^2(r)}{L^2}\,. \tag{27}$$

It is not very likely that condition (27) is satisfied and as a matter of fact there is not a lot of interest in that case. What is likely to happen is that there is at least one $n = n_0 \in N_0$ for which the range

$$[\frac{\pi n_0}{L}\min v_A(r) \;\;,\;\; \frac{\pi n_0}{L}\max v_A(r)]. \tag{28}$$

contains the driving frequency of the footpoint motion ω. In that case there is a position $r = r_A$, given by

$$\omega^2 = \frac{\pi^2 n_0^2 v_A^2(r_A)}{L^2} \tag{29}$$

where V_{n_0} (Eq. (25)) diverges. It is this resonant solution which blows up in ideal MHD that we are interested in and that we want to study in dissipative MHD. The resonant condition (29) is due to the finite extent of the cylinder in the longitudinal direction. The range of resonant frequencies (28) was found earlier by Halberstadt & Goedbloed (1995b).

In order to make the singularity in the ideal MHD solution for $V_{n_0}(r)$ clearly visible we use the linear Taylor polynomial of $\omega^2 - \pi^2 n_0^2 v_A^2(r)/L^2$ around the resonant point $r = r_A$:

$$\omega^2 - \pi^2 n_0^2 v_A^2(r)/L^2 = (r - r_A)\Delta + \cdots = s\Delta + \cdots\,, \tag{30}$$

where

$$\Delta = \frac{d}{dr}\left(\omega^2 - \frac{\pi^2 n_0^2 v_A^2}{L^2}\right)\Big|_{r=r_A}\,, \tag{31}$$

and $s = r - r_A$. We assume that this linear Taylor polynomial is an accurate approximation of the actual function in the interval $[r_A - s_A \;,\; r_A + s_A]$. The ideal MHD solution for $V_{n_0}(r)$ in the vicinity of the resonant point then takes the form

$$V_{n_0}(r) = \frac{-2\omega^2 f(r_A)}{\pi n_0 (r - r_A)\Delta} \tag{32}$$

which clearly shows that the ideal MHD solution for the resonant coefficient function $V_{n_0}(r)$ blows up as $1/(r - r_A)$. In what follows we assume that the resonant condition (29) occurs for at least one of the coefficient function for example that with index n_0. For the non-resonant coefficient functions the ideal solution given by Eq. (25) is an accurate solution in the whole r-domain. A slightly better solution can be obtained for these functions by

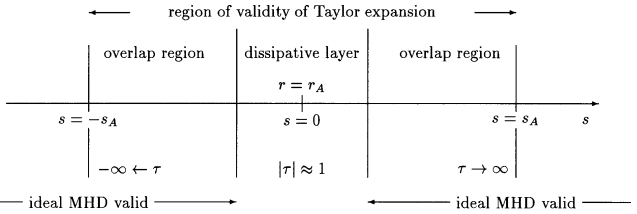

Fig. 1. A schematic overview of the notations used when treating the solution in the dissipative layer.

keeping the dissipative contribution in the right hand member but we shall show that $g(r) \approx -\omega^2 f(r)$ so that this operation is in fact irrelevant. For the resonant coefficient function $V_{n_0}(r)$ the ideal MHD solution (25) is accurate sufficiently far from the resonant point but is not valid close to the resonant point since dissipation plays an important role there.

3.3. Solution in a weakly dissipative plasma

In this section we obtain the dissipative solution for the coefficient function $V_{n_0}(r)$, that in ideal MHD diverges as $1/(r-r_A)$. So we focus on the dissipative Eq. (23) for $n = n_0$, which is valid everywhere and in particular in the vicinity of the resonant position $r = r_A$. Dissipation removes the ideal singularity from Eq. (23) and leads to the appearance of a thin dissipative layer embracing the ideal resonant surface. We will show that the very large Reynolds numbers in the solar corona imply that the thickness of the resonant layer δ_A is much smaller than the range of validity s_A of the Taylor expansion

$$\frac{\delta_A}{s_A} << 1 \,. \tag{33}$$

This inequality is important since it implies that in addition to the dissipative layer there are also two overlap regions to the left and the right of the dissipative layer contained in the interval $[r_A - s_A \,,\; r_A + s_A]$ (see Fig. 1).

The linear Taylor polynomial for the function $\omega^2 - \pi^2 n_0^2 v_A^2/L^2$ is now used to obtain a simplified version of Eq. (23) valid in the interval $|r - r_A| \lesssim s_A$

$$\Delta(r - r_A)V_{n_0} - i\omega(\nu + \eta)\frac{d^2 V_{n_0}(r)}{dr^2} = \frac{2}{\pi n_0} g(r) \,. \tag{34}$$

The second term in the left-hand side of Eq. (34) is due to dissipation. Dissipation plays a role of significance only when the second term is comparable in absolute value to the first term. This results in a dissipative layer of which the thickness is measured by the quantity

$$\delta_A = \left| \frac{\omega(\nu + \eta)}{\Delta} \right|^{1/3} \,. \tag{35}$$

In view of the very large values of the Reynolds numbers in the solar atmosphere, equation (35) implies that inequality (33) indeed holds.

Let us now consider the function $g(r)$ which appears in the right hand member of Eq. (34). In what follows we assume that the characteristic scale of variation of the driving function $f(r)$ is larger than or at least of the same order as δ_A. The ratio of the dissipative term in $g(r)$ to the actual driving term $f(r)$ can then be estimated as

$$\left| \frac{i\omega(\nu + \eta)}{\omega^2 f} \frac{d^2 f(r)}{dr^2} \right| \lesssim \frac{\delta_A |\Delta|}{\omega^2} \sim \frac{\delta_A}{l_{\rm eq}} \ll 1 \,, \tag{36}$$

where $l_{\rm eq}$ is the characteristic lengthscale for the variation of the physical quantities in the inhomogeneous equilibruim state. This estimate (36) shows that indeed

$$g(r) \approx -\omega^2 f(r) \,. \tag{37}$$

This implies that the ideal MHD solution (25) is valid for $n \neq n_0$ even in the peculiar case that the driving force is concentrated in a very narrow layer with the thickness of the order of δ_A.

Inspired by the analysis by Boris (1968), Kappraff & Tataronis (1977), Mok & Einaudi (1985) and Goossens et al. (1995), we introduce a new dimensionless variable $\tau = (r - r_A)/\delta_A$. This variable is of order 1 in the dissipative layer, and $r \rightarrow r_A \pm s_A$ correspond to $\tau \rightarrow \pm\infty$ (see Fig. 1). With this new variable we rewrite Eq. (34) as

$$\frac{d^2 V_{n_0}(\tau)}{d\tau^2} + i\tau V_{n_0}(\tau) \mathrm{sign}\Delta = -\frac{2i\omega^2}{\pi n_0 \delta_A |\Delta|} f(\tau) \,. \tag{38}$$

The dissipative solution for $V_{n_0}(\tau)$ takes a particular simple form in the realistic case that the characteristic scale of the driver is much larger than δ_A, so that we can take $f(\tau) \approx f(\tau = 0) = f(r = r_A) \equiv f_A$ in the dissipative layer. In that case the RHS of Eq. (38) is constant and it was shown in Goossens et al. (1995) that the solution, that does not diverge exponentially for $|\tau| \rightarrow \infty$, is given by

$$V_{n_0}(\tau) = \frac{2i\omega^2 f_A}{\pi n_0 \delta_A |\Delta|} F(\tau) \,, \tag{39}$$

where $F(\tau)$ is the universal function which was first introduced by Boris (1968)

$$F(\tau) = \int_0^\infty \exp(ik\tau \mathrm{sign}\Delta - k^3/3)\, dk \,. \tag{40}$$

Goossens et al. (1995) used this function in their analytical study of linear resonant Alfvén waves in flux tubes that are excited by lateral driving. Wright & Allan (1996) showed in a study on resonant Alfvén waves in magnetospheric conditions that the analytical structure embodied in this function is fairly insensitive to the details of the dissipation mechanism. The term 'universal function' is therefore appropiate. For completeness we obtain in the appendix the solution to Eq. (38) without making any further assumption about the function $f(\tau)$ other than the one we need to arrive at the Eq. (38). This solution covers driving profiles $f(\tau)$ with variations down to the scale of δ_A so that even very localised photospheric perturbations are included.

Let us compare the amplitude of the oscillations associated with the coefficient function $V_{n_0}(r)$ respectively in dissipative layer and far away from the dissipative layer for a driver that has the same amplitude in the dissipative layer and far away from the dissipative layer. In that case the characteristic scale of driver is much larger than δ_A and we can use the expression (39) in the dissipative layer. With the result that $F(0) = 3^{-2/3}\Gamma(1/3) \approx 1.29$ where Γ is the gamma-function, we find that the amplitude of oscillation in the centre of the dissipative layer ($\tau = 0$) is

$$|V_{n_0}(0)| \approx 0.82 \frac{\omega^2 f_A}{n_0 \delta_A |\Delta|} . \tag{41}$$

Far away from the dissipative layer V_{n_0} is given by Eq. (25). If we assume that $|\omega^2 - \pi^2 n_0^2 v_A^2| \sim \omega^2$ far away from the dissipative layer we obtain

$$|V_{n_0}| \sim \frac{2}{\pi n_0} f_A . \tag{42}$$

Eq. (41) and (42) show that the ratio of the amplitude in the dissipative layer to the amplitude far away from the dissipative layer is of the order of

$$\frac{l_{\rm eq}}{\delta_A} >> 1 . \tag{43}$$

This implies that the resonant Alfvén wave is indeed confined to a narrow dissipative region and that the dissipative coupling of the resonant magnetic surface is restricted to the immediate neighbourhood of the resonant surface. The solution in the planar geometry can be obtained by simple substitution.

3.4. Validity of the steady state approach

In the previous sections we assumed that the footpoint motion has driven the loop for a sufficiently long timespan in order for a steady state to be attained in which all perturbed quantities oscillate with the driving frequency ω. In this subsection we argue that this stationary situation is indeed attained after a realistic timespan.

The amplitude of the stationary dissipative solution at the resonant layer ($\tau = 0$) is given by (41), which can be rewritten as

$$|v_\varphi| \approx 1.20 f_A R^{1/3} \left(\frac{l_{eq}}{L}\right)^{1/3} , \tag{44}$$

where we use the notation $R = l_{eq} v_A/(\eta + \nu)$ for the Reynolds number and $\omega = n_0 \pi v_A/L$, with $n_0 = 1$. To prove that a stationary dissipative layer can be attained we have to show that the *time dependent* dissipative solution approaches the value (44) on a time scale smaller than the life time of the loop.

Unfortunately, the time-dependent dissipative solution is unknown. In an initial stage however, when small length scales did not develop yet, this time-dependent dissipative solution will be very close to the time-dependent *ideal* solution. Berghmans & De Bruyne (1995) showed that at the resonance the time-dependent ideal solution grows linearly in time

$$v_\varphi = f_A \frac{t}{T_A} , \tag{45}$$

where $T_A = L/v_A$ is the Alfvénic crossing time.

Although the growth of the time-dependent dissipative solution will be slower than linear after some time and will approach the stationary value (44), it seems fair to estimate the time needed in order to reach the asymptotic state T_{as} as the time needed for (45) to grow up to the level (44). This results in

$$T_{as} = 1.20\ R^{1/3} \left(\frac{l_{eq}}{L}\right)^{1/3} T_A . \tag{46}$$

For the parameters given by Beaufumeé, Coppi and Golub (1992) for an intermediate loop (their table 2, loop 2) this results in $T_{as} = 4.6\ R^{1/3}$ seconds. This means that for typical coronal values of the Reynold number (10^{10}-10^{12}), the stationary state is reached on a time scale of the order of a few hours. Hence, the characteristic time for building up the resonance layer is much smaller than the typical lifetime of a loop and a stationary approach is possible.

4. Energetics

In this section we calculate the energy dissipated in the coronal loop. As the z component of the velocity is equal to zero at $z = 0$, the energy flux through the surface $z = 0$ is given by the z-component of the Poynting vector $\mathbf{E} \times \mathbf{B}/\mu$ integrated over this surface. With the use of Ohm's and Ampere's laws we easily get

$$\frac{1}{\mu}\mathbf{E} \times \mathbf{B} = \frac{1}{\mu}[\mathbf{v}B^2 - \mathbf{B}(\mathbf{v} \cdot \mathbf{B})] + \frac{\eta}{\mu}(\nabla \times \mathbf{B}) \times \mathbf{B} . \tag{47}$$

Taking into account that only the $\varphi-$components of the velocity and the perturbed magnetic field differ from zero, we obtain

$$\frac{1}{\mu}(\mathbf{E} \times \mathbf{B})_z = -\frac{1}{\mu} B_0 v_\varphi B'_\varphi - \frac{\eta}{\mu} B'_\varphi \frac{\partial B'_\varphi}{\partial z} . \tag{48}$$

In what follows we denote the magnetic Reynolds number as R_m. The ratio of the second term in the right-hand side of Eq. (48) to the first term is of the order of $\eta/v_A L = R_m^{-1}$ both inside and outside the dissipative layer. Since $R_m \gg 1$, this estimate enables us to neglect the second term in the right-hand side of equation (48) in comparison with the first term. The $z-$component of the instantaneous Poynting flux $S(t)$ can then be written as

$$S(t) = -\frac{2\pi}{\mu} \int_0^\infty B_0 v_\varphi B'_\varphi r\, dr . \tag{49}$$

The quantities v_φ and B'_φ in Eq. (49) are calculated at $z = 0$.

Let us now use the analytic solution obtained in the previous section for calculating $S(t)$. The quantity v_φ is defined by the boundary condition (14a). We use Eq. (11) in order to find B'_φ.

It is straightforward to show that the ratio of the second term in the right-hand side of Eq. (11) to the first term is of the order R_m^{-1} far away from the dissipative layer, and of the order $R_m^{-1/3}$ in the dissipative layer. This observation enables us to neglect the second term in comparison with the first term. With the use of Eqs. (17) and (21) which determine the solution for v_φ, we obtain from equation (11) that

$$B'_\varphi = \frac{iB_0}{\omega L}\left\{\pi\sum_{n=1}^{\infty} nV_n(r)\cos\frac{\pi nz}{L} - f(r)\right\} . \quad (50)$$

When looking for a solution proportional to $e^{-i\omega t}$, we implicitly assumed that the solution is of the form $q(t,r,z) = Re[q(r,z)e^{-i\omega t}]$, where q is any perturbed quantity. Therefore, when calculating $S(t)$, we need to evaluate (50) at $z = 0$, multiply it by $e^{-i\omega t}$ and substitute the real part of the result into Eq. (49). Similarly we have to substitute $v_\varphi = Re[f(r)e^{-i\omega t}]$. In what follows we take $f(r)$ to be a real function. This means that at the footpoint ($z = 0$) all magnetic surfaces $r = \text{const}$ oscillate synchronously, i.e. there are no phase shifts between the oscillations of different magnetic surfaces. The choice of a complex function $f(r)$ would allow us to introduce phase shifts between different magnetic surfaces. We can split the instantaneous Poynting flux $S(t)$ in a constant part $S_{\rm con}$ and an oscillatory part $S_{\rm osc}$

$$S(t) = S_{\rm con} + S_{\rm osc}(t) , \quad (51)$$

where

$$S_{\rm con} = \frac{\pi^2}{\omega L}\int_0^\infty \rho_0 v_A^2 f(r)\sum_{n=1}^{\infty} nV_n^{(i)} r\,dr , \quad (52)$$

$$S_{\rm osc}(t) = \frac{\pi}{\omega L}\sin 2\omega t\int_0^\infty \rho_0 v_A^2 f(r)\left\{f(r) - \pi\sum_{n=1}^{\infty} nV_n^{(r)}\right\} r\,dr + \frac{\pi^2}{\omega L}\cos 2\omega t\int_0^\infty \rho_0 v_A^2 f(r)\sum_{n=1}^{\infty} nV_n^{(i)} r\,dr , \quad (53)$$

and $V_n^{(r)}$ and $V_n^{(i)}$ are the real and imaginary parts of the quantity V_n.

It is instructive to use the analogy with an electrical circuit for the interpretation of the formulae (51)-(53). In this picture we view a coronal loop as a loading, and the driver as an electromotive force. In general the coronal loop is partly an active and partly a reactive loading. The mean value of $S_{\rm osc}(t)$ over a period is zero, so that $S_{\rm osc}(t)$ describes the energetics of the reactive part of the loading. In contrast, $S_{\rm con}$ describes the energetics of the active part of the loading.

In accordance with Eq. (25) $V_n^{(i)} = 0$ everywhere for $n \neq n_0$, and $V_{n_0}^{(i)} = 0$ away from the dissipative layer. We substitute $r = \delta_A\tau$ into Eq. (52) to arrive at

$$S_{\rm con} = \frac{\pi^2 r_A\rho_0 v_A^2\delta_A}{\omega L}\int_{-\infty}^{\infty} f(\tau)V_{n_0}^{(i)}(\tau)\,d\tau . \quad (54)$$

In Eq. (54) ρ_0 and v_A are calculated at $r = r_A$ and the function $V_{n_0}^{(i)}$ is given by the expression (A7). The substitution of this expression in Eq. (54) results in

$$S_{\rm con} = \frac{2\pi^{1/2}\omega r_A\rho_0 v_A^2}{n_0 L|\Delta|} Re\left\{\iint_{-\infty}^{\infty} Q(\tau,\bar\tau)f(\tau)f(\bar\tau)\,d\tau\,d\bar\tau\right\} . \quad (55)$$

This expression together with the expression (A8) for the function $Q(\tau,\bar\tau)$ clearly shows that the quantity $S_{\rm con}$ is independent of the dissipative coefficients ν and η, which means that the amount of dissipated energy is independent of the actual dissipation mechanism.

Let us multiply Eq. (38) by $V_{n_0}^*$, where an asterisk denotes a complex conjugated value, and integrate with respect to τ. Since $f(\tau)$ is real by assumption, we obtain

$$\int_{-\infty}^{\infty} f(\tau)V_{n_0}^{(i)}(\tau)\,d\tau = \frac{n_0\pi\delta_A|\Delta|}{2\omega^2}\int_{-\infty}^{\infty}\left|\frac{dV_{n_0}}{d\tau}\right|^2 d\tau . \quad (56)$$

Substitution of Eq. (56) into Eq. (54) gives

$$S_{\rm con} = \frac{n_0\pi^3 r_A\rho_0 v_A^2\delta_A^2|\Delta|}{2\omega^3 L}\int_{-\infty}^{\infty}\left|\frac{dV_{n_0}}{d\tau}\right|^2 d\tau . \quad (57)$$

Eq. (57) implies that $S_{\rm con} > 0$ as can be expected from a physical point of view.

The expression for $S_{\rm con}$ takes an especially simple form when $f(\tau) \approx f_A$ in the dissipative layer:

$$S_{\rm con} = \frac{2\pi^2\omega r_A\rho_0 v_A^2 f_A^2}{n_0 L|\Delta|} . \quad (58)$$

The Poynting energy flux averaged over a period is equal to zero away from the dissipative layer. Therefore the two parts of the coronal loop that are to the left and to the right of the dissipative layer behave as a purely reactive loading. This result is what we could anticipate because we neglect dissipation away from the dissipative layer. In contrast, in the dissipative layer the average Poynting energy flux is non-zero, so that the dissipative layer behaves as partly reactive and partly active loading.

5. Comparison with numerical solution

The analysis of Sects. 3 and 4 has given us a straightforward physical characterization of the resonant Alfvén waves. A key point of the analytic discussion was the use of the simplified dissipative MHD equation (38) for the resonant coefficient function. This equation was obtained by replacing the function $\omega^2 - \pi^2 n_0^2 v_A^2/L^2$ with its linear Taylor polynomial. The solution to this simplified dissipative MHD equation is obtained in closed analytic form (A7). The combination of the analytic solution to this simplified dissipative MHD equation and the analytic solution to the ideal MHD equations provides us with the full solution for the resonant Alfvén waves. From a computational point of view the use of this analytical solution is almost trivial compared to a sophisticated code which solves the full set

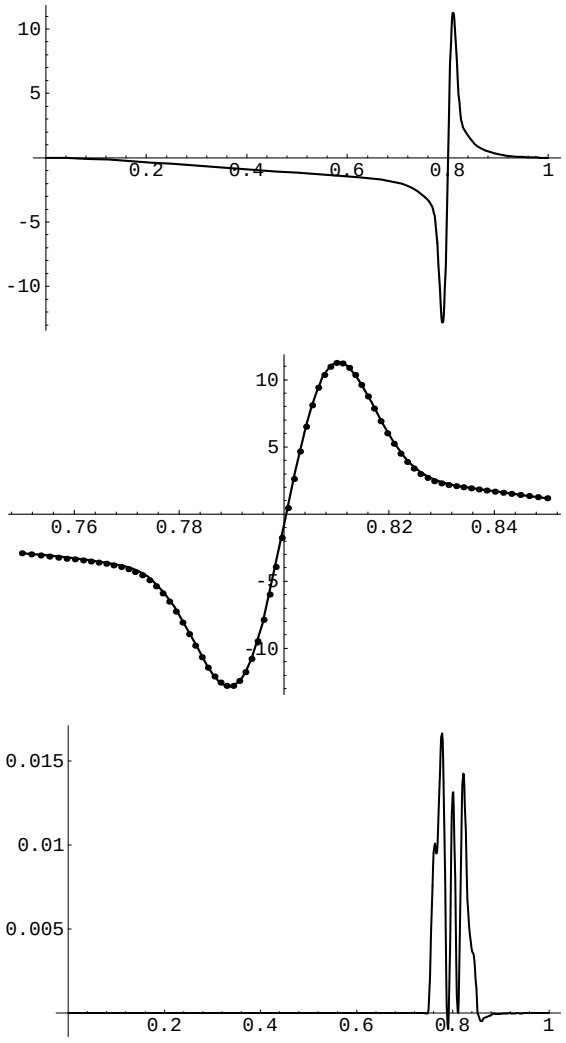

Fig. 2. Real part of $v_\varphi(r,z)$ as a function of r at $z = L/2$ over the whole interval(top), in the dissipative layer (middle) and the relative differences (bottom).

of linear non-ideal MHD equations in the whole volume of the equilibrium state. However if we want to use the present analytic solutions for an accurate determination of resonant Alfvén waves, we have to find out how good an approximation the analytical solution (A7) is to the original set of dissipative MHD equations. This situation is similar to that considered by Stenuit et al. (1995). These authors verified the accuracy of the analytic solutions to the simplified dissipative MHD equations for lateral driving. They found that the relative differences for the absorption coefficient was always smaller than 0.2%.

The test example for comparing results obtained with the present analytic theory with results obtained by numerical integration of the linear resistive MHD equations consists of an equilibrium state specified by

$$B_0 = \text{constant}\,, \quad \rho_0(r) = \rho_{00}\left(1 - \frac{4r^2}{5a^2}\right)\,, \tag{59}$$

where a is the radius of a magnetic tube, and $\rho_{00} = \rho_0(0)$, and a driver

$$f(r) = 16 f_0 \left(\frac{r}{a}\right)^2 \left(1 - \frac{r}{a}\right)^2\,, \tag{60}$$

with maximal amplitude $f_0 = f(a/2)$. The length of the magnetic tube L is taken to be $L = 4a$. The driving frequency ω is chosen so that the Alfvén resonance occurs for the first harmonic at the position $r_A = 0.8a$. This leads to

$$\omega = \frac{5\pi v_{A0}}{4a}\sqrt{\frac{5}{61}} \approx 1.124\frac{v_{A0}}{a} \quad \wedge \quad f_A = 0.4096 f_0\,, \tag{61}$$

where $v_{A0} = v_A(0)$. In the present equilibrium model the radius a of the magnetic tube is a good choice for the characteristic length scale of the inhomogeneous equilibrium state l_{eq}. The magnetic Reynolds number is taken to be $R_m \equiv a v_{A0}/\eta = 10^6$.

The numerical simulation uses a finite element discretization in the radial direction and a Fourier decomposition in the longitudinal direction. The results of the numerical simulation are for 201 grid points in the radial direction and for 11 complex Fourier terms $\exp(\pi i n z/L)$ with n from -5 to 5 in the longitudinal direction. In order to have a better resolution of the solutions in the dissipative layer mesh accumulation is used there with about 75 mesh points in the interval from 0.75 to 0.85.

First we compare the values for the Pointing energy flux averaged over a period. The value found for $S_{\rm con}$ in the numerical simulation where the resistive MHD equations are integrated over the whole volume of the loop is $S_{\rm con} \approx 0.2244\,\rho_{00} v_{A0} a^2 f_0^2$. The fourth decimal cannot be guaranteed since the Poynting flux through the upper boundary at $z = L$, which is zero, is found to be $0.0003\,\rho_{00} v_{A0} a^2 f_0^2$ in the numerical simulation. The value obtained with the present analytic theory is

$$\begin{aligned} S_{\rm con} &= \frac{\pi}{125}\left(\frac{4}{5}\right)^7\left(\frac{61}{5}\right)^{3/2}\rho_{00} v_{A0} a^2 f_0^2 \\ &\approx 0.2245\,\rho_{00} v_{A0} a^2 f_0^2 \end{aligned} \tag{62}$$

when expression (58) is used as a first approximation for computing $S_{\rm con}$ and $S_{\rm con} \approx 0.2247\,\rho_{00} v_{A0} a^2 f_0^2$ when the more accurate analytical expression (54) is evaluated. The three values for $S_{\rm con}$ have three common decimals. This is a remarkably good agreement. It is also surprising that expression (58) provides such a good approximation although the characteristic scale of the driver is not very much larger than the length scale defined by δ_A in the present application.

Figs. 2 and 3 show the variations of the real and imaginary parts of $v_\varphi(r,z)$ as functions of the radial coordinate r at fixed height $z = L/2$. These two figures each consist of three parts. The upper part shows the analytical solutions over the whole radial interval. The analytic solution for the real part of $v_\varphi(r,z)$ is computed with the exact expression (26) outside the dissipative layer and using 10 Fourier terms with their corresponding ideal coefficient functions $V_n(r)$ $n \neq 1$ and the analytic dissipative solution $V_1(\tau)$ given by (A7) in the dissipative layer. Apparently

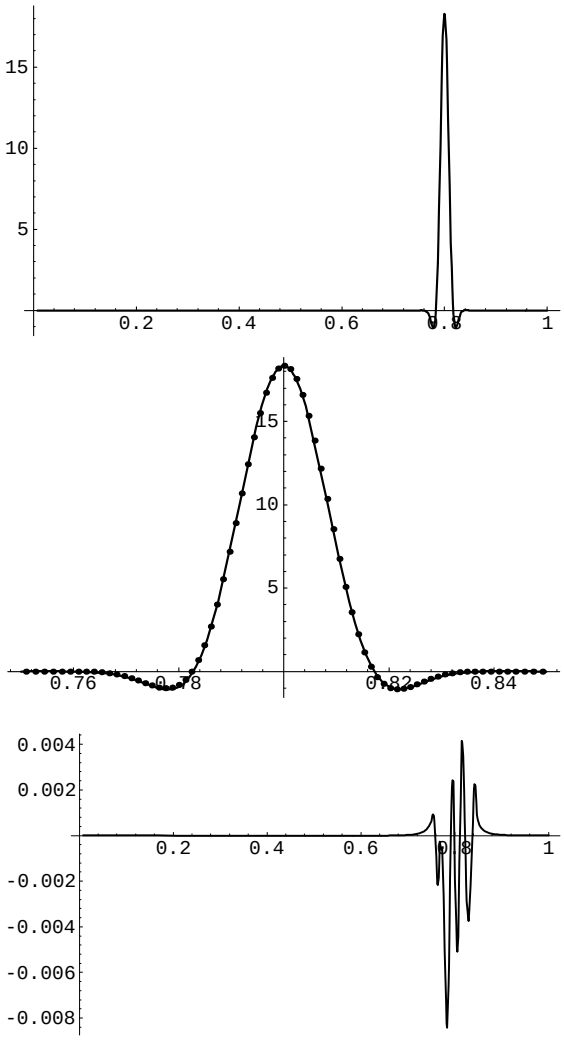

Fig. 3. Imaginary part of $v_\varphi(r,z)$ as a function of r at $z = L/2$ over the whole interval (top), in the dissipative layer (middle) and the relative differences (bottom).

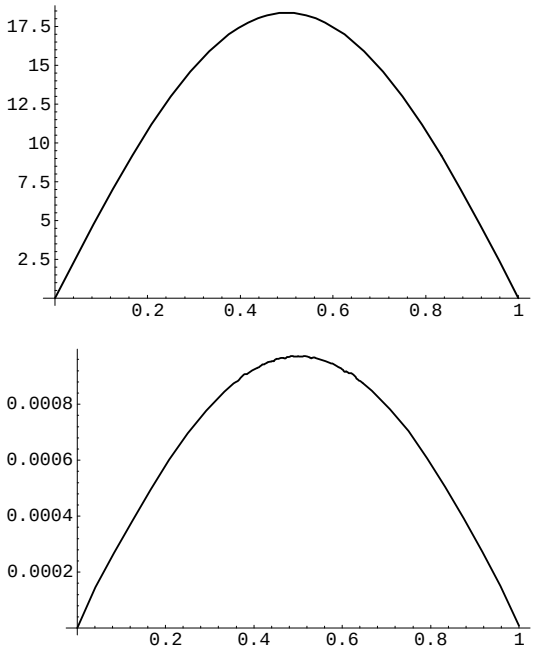

Fig. 4. Imaginary part of $v_\varphi(r,z)$ as a function of z at $r = 0.8a$ i.e. in the dissipative layer (top), and the relative differences (bottom).

the number of Fourier terms corresponding to ideal coefficient functions $V_n(r)$ $n \neq 1$ has not any noticeable effect on the solution in the dissipative layer. The analytic solution for the imaginary part of $v_\varphi(r,z)$ is computed with one Fourier term $n = 1$ and the analytic dissipative solution $V_1(\tau)$ given by (A7) in the dissipative layer. The imaginary parts of the coefficient functions with $n \neq 1$ are identically zero.

The differences between the analytical and the numerical solution are invisible on the scales used on the upper parts of figures 2 and 3. The real part of the solution is characterized by the remnant of the ideal $1/(r - r_A)$ singularity, while the imaginary part is dominated by the remnant of the ideal $\delta-$ function. The middle part gives an enlarged view of the solution in the dissipative layer which here covers the interval from 0.75 to 0.85. The analytical solution is represented by the full line, while the dots are the results of the numerical simulation. Here also the differences between the analytic and numeric results are invisible. The lower part shows the relative differences between the analytic and numeric results, more precisely we have plotted (analytic result - numeric result)/ (largest absolute value of the analytic results). Outside the dissipative layer the analytic and numeric results are identical. Inside the dissipative layer the relative differences are in absolute value smaller than 2% for the real part and 1% for the imaginary part. This is of course an excellent agreement. It is not obvious whether these small differences are primarily due to the approximations used in the analytic theory in order to obtain an analytic solution in the dissipative layer or to inaccuracies in the numeric simulation. The relative difference of the imaginary part of v_φ is a rapidly oscillating function around zero and in absolute value always smaller than 1%. This explains the remarkably good agreement for $S_{\rm con}$ since according to (54) $S_{\rm con}$ is the integral of $V_{n_0}(\tau)$ multiplied with $f(\tau)$ over τ.

Figs. 4 and 5 show the variation of the imaginary part of $v_\varphi(r,z)$ at the resonant position in the dissipative layer ($r = r_A = 0.8a$) and of the real part of v_φ far away from the dissipative layer ($r = 0.5a$) as functions of z. The ratio of the real part of $v_\varphi(r,z)$ to the imaginary part is of the order of $\delta_A/a \ll 1$ at $r = 0.8a$, and the imaginary part of $v_\varphi(r,z)$ is zero everywhere outside the dissipative layer and, in particular, at $r = 0.5a$. Figs. 4 and 5 consist of two parts. The upper part shows the analytic solution, while the lower part shows the relative differences. The analytic solution of the imaginary part of $v_\varphi(r,z)$ at the resonant position is computed with one Fourier term $n = 1$ and the analytic dissipative solution $V_1(\tau)$ given by (A7) evaluated at $\tau = 0$. The imaginary parts of the coefficient functions with $n \neq 1$ are identically zero. The analytic

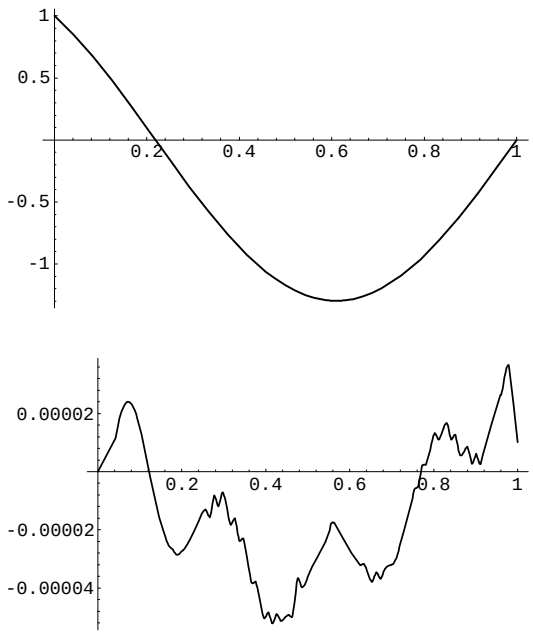

Fig. 5. Real part of $v_\varphi(r,z)$ as a function of z at $r = 0.5a$ i.e. far away from the dissipative layer (top), and the relative differences (bottom).

solution for the real part of $v_\varphi(r,z)$ is computed with the exact expression (26) since we are outside the dissipative layer. The differences in the imaginary part of $v_\varphi(r,z)$ are due to the difference present in Fig. 3 at $\tau = 0$ which now shows up as the amplitude in the variation of the relative difference as a function of z. The agreement is remarkably good with the relative differences all being smaller than 0.1%. The differences in the real part of $v_\varphi(r,z)$ are due to inaccuracies in the solution of the numerical simulation and are of the order of 0.00005 in absolute values. Errors of the same size are present in the solution of the numerical simulation for the imaginary part of $v_\varphi(r,z)$ outside the dissipative layer where it should be zero. Again the agreement between the analytic and numeric results is excellent. The present analytic theory provides a simple means for a very accurate computation of resonant Alfvén waves.

6. Application to coronal loops

Let us now see how the results of the present paper can be related to observations of magnetic loops in the solar corona. Before we embark on a discussion where theoretical values of the flux of energy are compared with the required volumetric heating rates as inferred from observations, let us put the present theoretical results in a clear perspective. Our results were obtained for a very particular and limited subclass of motions in the solar photosphere. These motions have been driven at a single frequency giving rise to dissipation in just one thin dissipative layer. It is obvious that this set-up cannot provide the required volumetric heating rate. It would be very worrying if this would actually be the case. Only a tiny fraction of the kinetic energy in the photosphere is in purely azimuthal motions and driving does not occur at a single frequency but over a whole interval of frequencies.

Let us first see what we would get if we take the naive approach that a resonant torsional Alfvén wave with a single frequency heats a whole coronal loop. We adopt the classification of loops by Beaufumé et al. (1992) in a short dense loop (type 1), a medium one (type 2), and a longer one (type 3) and apply our results to these three cases. The results are for an quilibrium state and driver specified by Eqs. (59) and (60). However, in contrast to the previous section, we choose $r_A = a/2$, so that resonance takes place at the magnetic surface where the driver's amplitude is maximal.

As Beaufumé et al. (1992) give losses per unit volume we introduce the average Poynting energy flux per unit volume $S_{\rm con}/\mathscr{V}$, where $\mathscr{V} = \pi a^2 L$ is the loop volume. The approximate formula (58) for $S_{\rm con}$ leads to

$$S_{\rm con}/\mathscr{V} = 3.26 \times 10^{-11} B_0 n_e^{1/2} L^{-1} f_0^2 \ \ {\rm W\,m^{-3}}, \tag{63}$$

where n_e is the electron density at the magnetic loop axis and all quantities are measured in SI units. Eq. (63) holds for a resonance of the first harmonic ($n = 1$). The driving frequency corresponding to this resonance is

$$\omega = 6.85 \times 10^{16} B_0 n_e^{-1/2} L^{-1} \ \ {\rm s^{-1}}. \tag{64}$$

Beaufumé et al. (1992) give in their classification for type 1 loops $L = 2 \times 10^7$ m, $a = 4 \times 10^5$ m, $B_0 = 0.03$ Tesla, $n_e = 10^{16}$ m^{-3}, and the sum of radiative and conductive losses per unit volume $L_r + L_\kappa = 3.2 \times 10^{-3}$ W m^{-3}. Hence $\omega = 1.03$ s^{-1}, a wave period $P = 6.11$ s, and $S_{\rm con}/\mathscr{V} = 5.90 \times 10^{-12} f_0^2$ W m^{-3}. In order that the energy flux to the loop covers the losses one has to have $S_{\rm con}/\mathscr{V} = L_r + L_\kappa$ which results in the driver's amplitude $f_0 = 25.5$ km/s.

For type 2 loops Beaufumé et al. (1992) list $L = 6 \times 10^7$ m, $a = 1.2 \times 10^6$ m, $B_0 = 0.015$ Tesla, $n_e = 3 \times 10^{15}$ m^{-3}, and $L_r + L_\kappa = 2.4 \times 10^{-4}$ W m^{-3}. Hence $\omega = 0.313$ s^{-1}, $P = 20.1$ s, and $f_0 = 23.3$ km/s.

For type 3 loops Beaufumé et al. (1992) give $L = 2 \times 10^8$ m, $a = 4 \times 10^6$ m, $B_0 = 0.005$ Tesla, $n_e = 10^{15}$ m^{-3}, and $L_r + L_\kappa = 2.3 \times 10^{-5}$ W m^{-3}. These data lead to $\omega = 0.0542$ s^{-1}, $P = 116$ s, and $f_0 = 29.7$ km/s.

The periods are too short for type 1 and type 2 coronal loops. However there is the possibility that high-frequency motions in coronal loops are excited by low-frequency footpoint motions as discussed by Goedbloed (1994) and Poedts and Boynton (1996). The estimates for the driver's amplitude are quite resonable and generally in agreement with the observed values of the non-thermal velocities at the base of the solar corona. However the velocities in the dissipative layer, that correspond to these photospheric velocities, are larger by factor a/δ_A which is of the order of 100 even if we assume that turbulence reduces the viscous and magnetic Reynolds numbers to values of the order of 10^6. Such huge values of the non-thermal velocities have never been observed.

The reason for the difference between the values of velocities in the dissipative layer needed in the naive approach and the

observed non-thermal velocities is obvious. A magnetic loop is not heated by one resonant torsional Alfvén wave in just one dissipative layer. The footpoint motions have a range of frequencies which partly or even completely covers the range of resonant frequencies of the loop. In addition a lot of kinetic energy is available in other than purely azimuthal motions. If we approximate the continuous range of frequencies by the dicrete spectrum containing many frequencies, the whole volume of the loop is covered by a set of dissipative layers, each dissipative layer corresponding to one definite frequency of the discrete spectrum. In that case each Fourier component of the footpoint motion corresponding to a discrete frequency has to heat only plasma in the corresponding dissipative layer and its immediate vicinity.

Let us estimate the number of discrete frequencies and corresponding dissipative layers needed in order to obtain velocities in the dissipative layer of the order of 20 – 30 km/s. The ratio of the velocity in the dissipative layer to the photospheric velocity is of the order of a/δ_A. This implies that the driver's amplitude has to be of the order of $(\delta_A/a)\times(20 - 30$ km/s). Since the energy input is proportional to the square of driver's amplitude, this means that the motion which such an amplitude can cover only losses of $(\delta_A/a)^2$ part of the loop. Therefore in order to cover losses of the whole loop their needs to be a number of distinct frequencies of the order of $(a/\delta_A)^2$. This implies that the distances between the centres of the two neighbouring dissipative layers has to be of the order of δ_A^2/a. Since the thickness of the dissipative layers is of the order of δ_A, there is a very strong overlap of the dissipative layers. The analysis carried out in the present paper is not applicable to this situation. A new problem with the footpoint motion containing a continuous range of frequencies has to be solved in order to provide a more realistic picture of coronal loop heating.

7. Conclusions

The present paper has considered linear resonant Alfvén oscillations driven by the footpoint motions of the magnetic field lines in a coronal loop. The coronal loop is idealized as a straight one-dimensional magnetic cylinder of finite longitudinal extent in which the equilibrium quantities depend on the radial coordinate only. The analysis has been restricted to steady state of Alfvén waves driven by footpoint motions that are periodic in time, axially symmetric, and torsionally polarised. The solution for the Alfvén oscillations has been given as an infinite Fourier series with respect to the longitudinal coordinate. The focus has been on footpoint motions with frequencies that satisfy a resonant condition for the n_0-th harmonic of the Alfvén oscillations. In ideal MHD the spatial solution for this resonant harmonic blows up as $1/(r-r_A)$. Inclusion of dissipation removes this singularity. The fact that the viscous and magnetic Reynolds numbers are very large in the solar atmosphere has motivated us to use series expansions of the coefficient functions (in the dissipative MHD) around the ideal resonant position in order to obtain a simplified version of the set of the linear dissipative MHD equations. This simplified version is valid in the thin dissipative layer which embraces the ideal resonant position and in two overlap regions to the left and the right of the dissipative layer and allows a straightforward analytical solution. The combination of the analytical dissipative solution in the dissipative layer and the analytical ideal solution outside the dissipative layer gives us a complete analytical solution describing resonant Alfvén waves driven by footpoint motions. This analytical solution allows a straightforward physical and mathematical interpretation of linear resonant Alfvén waves. In addition, comparison with solution obtained by numerical integration of the linear resistive MHD equations in the whole volume shows that the analytic solution makes possible a very accurate computation of all physical quantities related to the resonant Alfvén waves with relatively little effort.

The present results are applied to the magnetic loops observed in the solar corona. It is shown that the energy of resonant Alfvén waves, absorbed in a coronal loop, covers radiative and conductive losses if the amplitude of the driving footpoint motions is of the order 20 – 30 km/s.

Acknowledgements. The authors thank J.L.Ballester for his suggestion to include the application of theoretical results to the observed coronal loops. This work was carried out while M.Ruderman was a guest at the K.U.Leuven. M.Ruderman acknowledges financial support by the 'Onderzoeksfonds K.U.Leuven' which made his fruitful and pleasant stay at the K.U.Leuven possible, and the warm hospitality of the Centre for Plasma Astrophysics of the K.U.Leuven.

Appendix A: general case

In this appendix we solve Eq. (38) for arbitrary driving profiles $f(\tau)$. The only limitation is that assumption (36) excludes driving profiles with radial variations below the (extremely small) scale δ_A. This is not really a restriction as the scale δ_A is very small so that the present analysis includes very localised photospheric perturbations.

The solution to Eq. (38) has to be matched to the ideal solution which is valid for $|\tau| >> 1$. This solution is given by Eq. (25) which rewritten in terms of the new variable τ takes the form

$$V_{n_0}(\tau) = -\frac{2\omega^2 f(\tau)}{\pi n_0 \delta_A \tau \Delta} . \tag{A1}$$

The matching principle requires that in the overlap region the asymptotic version for $\tau \to \infty$ of the solution to the dissipative equation (38) coincides with the ideal solution (25). This implies in particular that $V_{n_0}(\tau)$ vanishes at infinity and consequently that the Fourier transform of V_{n_0}

$$\hat{V}_{n_0}(k) = \int_{-\infty}^{\infty} V_{n_0}(\tau) e^{-i\tau k} d\tau , \tag{A2}$$

exists. Fourier transformation of Eq. (38) gives

$$\frac{d\hat{V}_{n_0}}{dk} + k^2 \hat{V}_{n_0} \mathrm{sign}\Delta = \frac{2i\omega^2}{n_0 \pi \delta_A \Delta} \hat{f} . \tag{A3}$$

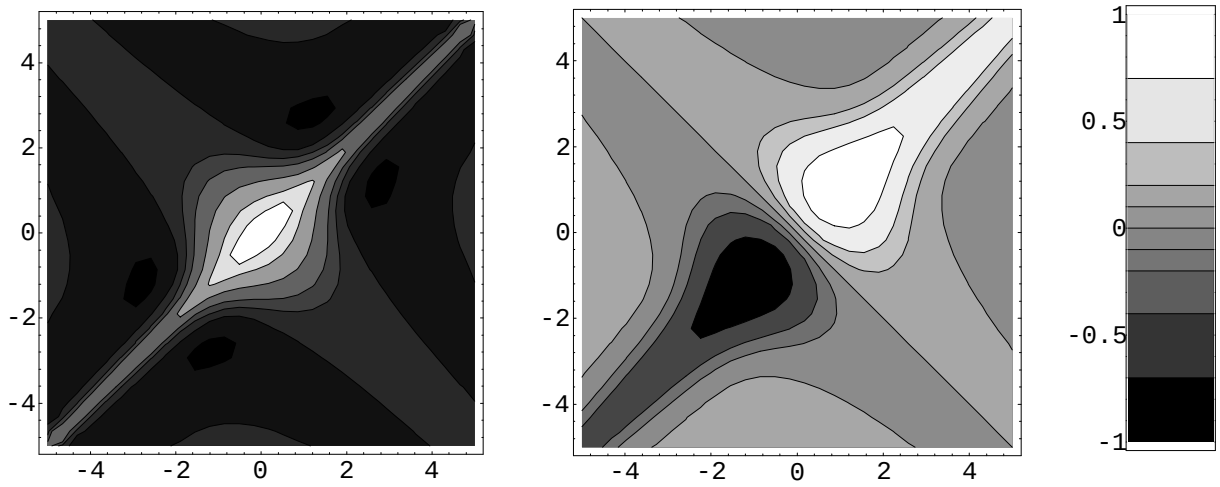

Fig. 6. Contourplots of the real (left) and imaginary (right) part of the kernel $Q(\tau,\bar{\tau})$ as a function of τ (horizontal axis) and $\bar{\tau}$ (vertical axis).

The solution to Eq. (A3) that vanishes at infinity is

$$\hat{V}_{n_0} = \frac{2i\omega^2}{n_0\pi\delta_A\Delta}\int_{\pm\infty}^{k}\hat{f}(\bar{k})\exp[(\bar{k}^3-k^3)\mathrm{sign}\Delta/3]\,d\bar{k}\,. \quad \text{(A4)}$$

The sign of the lower limit in the integral is $-$ for $\Delta>0$ and $+$ for $\Delta<0$. The expression (A4) can be rewritten as

$$\hat{V}_{n_0} = \frac{2i\omega^2}{n_0\pi\delta_A\Delta}\int_{-\infty}^{\infty}f(\bar{\tau})\,d\bar{\tau}\times \times\int_{\pm\infty}^{k}\exp[-i\bar{\tau}\bar{k}+(\bar{k}^3-k^3)\mathrm{sign}\Delta/3]\,d\bar{k}\,. \quad \text{(A5)}$$

The inverse Fourier transformation of $\hat{V}_{n_0}(\tau)$ gives

$$V_{n_0} = \frac{i\omega^2}{n_0\pi^2\delta_A\Delta}\int_{-\infty}^{\infty}f(\bar{\tau})\,d\bar{\tau}\int_{-\infty}^{\infty}e^{ik(\tau-\bar{\tau})}dk\times \times\int_{\pm\infty}^{0}\exp[-i\bar{\tau}\bar{k}+\bar{k}(k^2+k\bar{k}+\bar{k}^2/3)\mathrm{sign}\Delta]\,d\bar{k}\,. \quad \text{(A6)}$$

When deriving (A6) we used a change of variable from $\bar{k}$ into $k+\bar{k}$. A change of the order of integration results into

$$V_{n_0}(\tau) = \frac{2i\omega^2}{n_0\pi^{3/2}\delta_A|\Delta|}\int_{-\infty}^{\infty}Q(\tau,\bar{\tau})f(\bar{\tau})\,d\bar{\tau}\,, \quad \text{(A7)}$$

where

$$Q(\tau,\bar{\tau}) = \int_0^{\infty}\exp\left\{\frac{ik^2}{2}(\tau+\bar{\tau})\mathrm{sign}\Delta-\frac{k^6}{12}-\frac{(\tau-\bar{\tau})^2}{4k^2}\right\}dk. \quad \text{(A8)}$$

The kernel $Q(\tau,\bar{\tau})$ expresses the effect of a perturbation with unit amplitude located at $\bar{\tau}$ on the the amplitude $V_{n_0}(\tau)$. In this sense $Q(\tau,\bar{\tau})$ embodies the dissipative coupling between the different magnetic surfaces as well as the influence of the resonance. In figure 6 we have plotted the real and imaginary part of the kernel $Q(\tau,\bar{\tau})$. As can be expected, the largest values occur along the diagonal $\tau=\bar{\tau}$: the largest amplitudes develop on the magnetic surfaces where the driving is applied. For a fixed $\bar{\tau}$ the width of the ridge can be estimated to be $\triangle\tau\sim 2$. This means that, due to dissipation, the magnetic surfaces are coupled over a distance $\triangle r\sim\delta_A$ to the left and to the right of a specific magnetic surface. In addition it transpires that around $\tau\sim\bar{\tau}\sim 0$ the presence of the resonance results in larger amplitudes.

It is straightforward to show that the solution (A7) for $f(\tau)=f_A$ reduces to expression (39) found in Sect. 3.3. Let us now show that the dissipative solution (A7) indeed can be matched to the ideal solution (A1) in the two overlap regions to the left and the right of the dissipative layer. This means that the asymptotic behaviour of the dissipative solution (A7) for $|\tau|\to\infty$ has to recover the ideal MHD result (A1). In order to do that we change the order of integration in the dissipative solution (A7), make a substitution of the integration variable $\bar{\tau}=\tau+2k\tilde{\tau}$, and then change the order of integration once again. These manipulations enable us to arrive at

$$V_{n_0}(\tau) = \frac{4i\omega^2}{n_0\pi^{3/2}\delta_A|\Delta|}\int_{-\infty}^{\infty}e^{-\tilde{\tau}^2}d\tilde{\tau}\int_0^{\infty}kf(\tau+2k\tilde{\tau})\times \times\exp[i(k^2\tau+k^3\tilde{\tau})\mathrm{sign}\Delta-k^6/12]\,dk\,. \quad \text{(A9)}$$

The asymptotic expansion for $V_{n_0}(\tau)$ can now be obtained by means of integration by parts

$$V_{n_0}(\tau) = -\frac{2\omega^2 f(\tau)}{n_0\pi\delta_A\tau\Delta}+\mathcal{O}(\tau^{-2})\,. \quad \text{(A10)}$$

The asymptotic expansion (A10) is valid for $|\tau|\to\infty$ and shows that the asymptotic behaviour of $V_{n_0}(\tau)$ far away from the dissipative layer is really given by the ideal MHD solution (25).

References

Beaufumé, P., Coppi, B., & Golub, L., 1992, ApJ, 393, 396.
Berghmans, D., & De Bruyne, P., 1995, ApJ, 453, 495.
Berghmans, D., De Bruyne, P., & Goossens, M., 1996, ApJ, 472, *to appear*.

Boris, J.P., 1968, 'Resistive modified normal modes of an inhomogeneous incompressible plasma', Ph.D. Thesis Princeton University, UMI Dissertation Services, Ann Arbor Michigan, p. 172.
Davila, J.M., 1987, ApJ, 317, 514.
Goedbloed, J.P., 1994, International Conference on Plasma Physics, in press.
Goedbloed, J.P. & Halberstadt G., 1994, A&A, 286, 275.
Goossens, M., 1991, in E.R.Priest and A.W.Hood (eds.),'MHD Waves and Wave Heating in Non-Uniform Plasmas', *Advaces in Solar System Magnetohydrodynamics*, Cambridge University Press, Cambridge, p. 135.
Goossens, M. & Ruderman, M.S., 1995, Phys. Scripta, T60, 171.
Goossens, M., Ruderman, M.S., & Hollweg, J.V., 1995, Solar Phys., 157, 75.
Halberstadt G. & Goedbloed, J.P., 1995a, A&A, 301, 559
Halberstadt G. & Goedbloed, J.P., 1995b, A&A, 301, 577
Heyvaerts, J. & Priest, E.R., 1983, A&A, 117, 220
Hollweg, J.V., 1990, Computer Phys. Rep., 12, 205.
Hollweg, J.V., 1991, in P.Ulmschneider, E.R.Priest and R.Rosner (eds.), 'Alfvén Waves', *Mechanisms of Chromospheric and Coronal Heating*, Springer-Verlag, Berlin, p. 423.
Ionson, J.A., 1978, ApJ, 226, 650.
Ionson, J.A., 1985, Solar Phys., 100, 289.
Kappraff, J.M., & Tataronis, J.A., 1977, J. Plasma Phys., 18, 209.
Kuperus, M., Ionson, J.A., & Spicer, D., 1981, Ann. Rev. Astron. Astrophys., 19, 7.
Mok, Y., & Einaudi, G., 1985, J. Plasma Phys., 33, 199.
Ofman, L., & Davila, J.M., 1995, J. Geophys. Res., 100, 23427.
Ofman, L., Davila, J.M. & Steinolfson, R.S, 1995, ApJ, 444, 471.
Poedts, S., & Boynton, G.C., 1996, A&A, 306, 610.
Poedts, S., Goossens, M. & Kerner, W., 1989, Solar Phys., 123, 83.
Sakurai, T., Goossens, M. & Hollweg, J.V. 1991, Solar Phys., 133, 227.
Steinolfson, R.S. & Davila, J.M. 1993, ApJ, 415, 354.
Stenuit, H., Erdélyi, R. & Goossens, M. 1995, Solar Phys., 161, 139.
Straus, H.R., & Lawson, W.S., 1989, ApJ, 346, 1035.
Tirry, W.J. & Goossens M., 1996, ApJ, 471, 501.
Wright, A.N. & Allan W., 1996, JGR, 101, 17399.

This article was processed by the author using Springer-Verlag LaTeX A&A style file *L-AA* version 3.